Physics of the Earth and Planetary Interiors 189 (2011) 80–91

Contents lists available at ScienceDirect

Physics of the Earth and Planetary Interiors

journal homepage: www.elsevier.com/locate/pepi

Rupture at the flank of the subducted Gagua ridge: The 18 December 2001 earthquake (Mw 6.8) offshore eastern Taiwan

K.I. Konstantinou [a,*], S.-J. Lee [b], Y. Font [c], H. Kao [d]

[a] Institute of Geophysics, National Central University, Taiwan
[b] Institute of Earth Sciences, Academia Sinica, Taiwan
[c] Geoazur, Villefranche-sur-Mer Cedex, France
[d] Geological Survey of Canada, Pacific Geoscience Center, British Columbia, Canada

ARTICLE INFO

Article history:
Received 5 January 2011
Received in revised form 30 June 2011
Accepted 11 July 2011
Available online 23 July 2011

Keywords:
Ryukyu subduction
Taiwan
Gagua ridge
Slip distribution
Seamount

ABSTRACT

The southern Ryukyus represents an area where different tectonic stress regimes result in high seismicity and increased seismic hazard for nearby areas such as Taiwan. On 18 December 2001 at 04:03 (GMT) a strong earthquake (Mw 6.8) occurred in the forearc area of the southern Ryukyu subduction zone. Revised moment tensor solutions published by GCMT and BATS groups show a normal faulting mechanism with some strike-slip component and also point to a shallow focal depth (~12 km). We use arrival times picked at both Taiwanese and Japanese stations along with a 3D geo-realistic *a priori* velocity model in order to obtain accurate absolute locations for the mainshock and 153 of its aftershocks. Locations are derived by using the Maximum intersection (MAXI) algorithm which has been used in many previous seismicity studies in the southern Ryukyus. These improved locations indicate that the mainshock was caused by the failure of a NE–SW oriented fault that extends from the edge of the Nanao forearc sedimentary basin to the Ryukyu arc basement. Far-field P and SH waveforms of the mainshock recorded at stations surrounding the source and at distances 30–100°, were inverted for the purpose of investigating its rupture process. A non-negative least-squares inversion technique utilizing multiple time windows was used to derive the spatio-temporal slip distribution. The preferred slip distribution model shows that there is one large area of high slip (~0.9 m) at 5–15 km depth that essentially represents the crystalline rocks of the Ryukyu arc basement. Another smaller area with lower slip (~0.4 m) extends at 10–15 km depth beneath the Nanao basin. Most aftershocks are located in areas of low slip (<0.4 m) filling the regions of slip deficit. It is likely that the 18 December 2001 earthquake was caused by a stress field interaction generated by the oblique subduction of the Gagua ridge and the gravitational forces acting at its landward flank.

1. Introduction

The Ryukyu subduction zone was formed from the movement of the Philippine Sea plate underneath the Eurasian plate at a present rate of 8.2 cm year^{-1} (Yu et al., 1997). This subduction system extends from Kyushu island in the north, initially with a strike in the NE–SW direction, to Taiwan in the south where the strike changes to E–W possibly due to the collision between the Luzon Arc and the Chinese continental shelf (Tsai, 1986; Wu et al., 1997) (Fig. 1). To the north of the subduction zone, the Okinawa trough is the back arc basin of the Ryukyu trench and is in the process of opening as has been demonstrated by GPS measurements in the Ryukyu islands (e.g., Nakamura, 2004) and normal faulting earthquakes occurring offshore NE Taiwan (Yeh et al., 1991; Kao and Jian, 2001; Kubo and Fukuyama, 2003).

The most prominent morphological feature on the subducting Philippine Sea plate near Taiwan is a 20–30 km wide and over 300 km long N–S trending ridge, called the Gagua ridge. Detailed geophysical and bathymetric studies of the Gagua ridge suggest that it may have been formed by the compression and uplift of an earlier fracture zone during a plate reorganization at Mid-Eocene (Deschamps et al., 1998). Furthermore, bathymetric and seafloor imaging studies around the area where the ridge intersects the Ryukyu trench indicate significant deformation in the form of fracture networks and seafloor uplift, which is interpreted as evidence that at least a part of the ridge has already been subducted (Dominguez et al., 1998). At the other side of the trench, the forearc area is characterized by the Ryukyu arc slope, a series of sedimentary basins, the accretionary complex

* Corresponding author. Address: Institute of Geophysics, National Central University, Jhongda Road, Jhongli 320, Taiwan. Fax: +886 3 422204.
E-mail addresses: kkonst@ncu.edu.tw (K.I. Konstantinou), sjlee@earth.sinica.edu.tw (S.-J. Lee), font@geoazur.obs-vlfr.fr (Y. Font), hkao@nrcan.gc.ca (H. Kao).

0031-9201/$ - see front matter © 2011 Elsevier B.V. All rights reserved.
doi:10.1016/j.pepi.2011.07.010

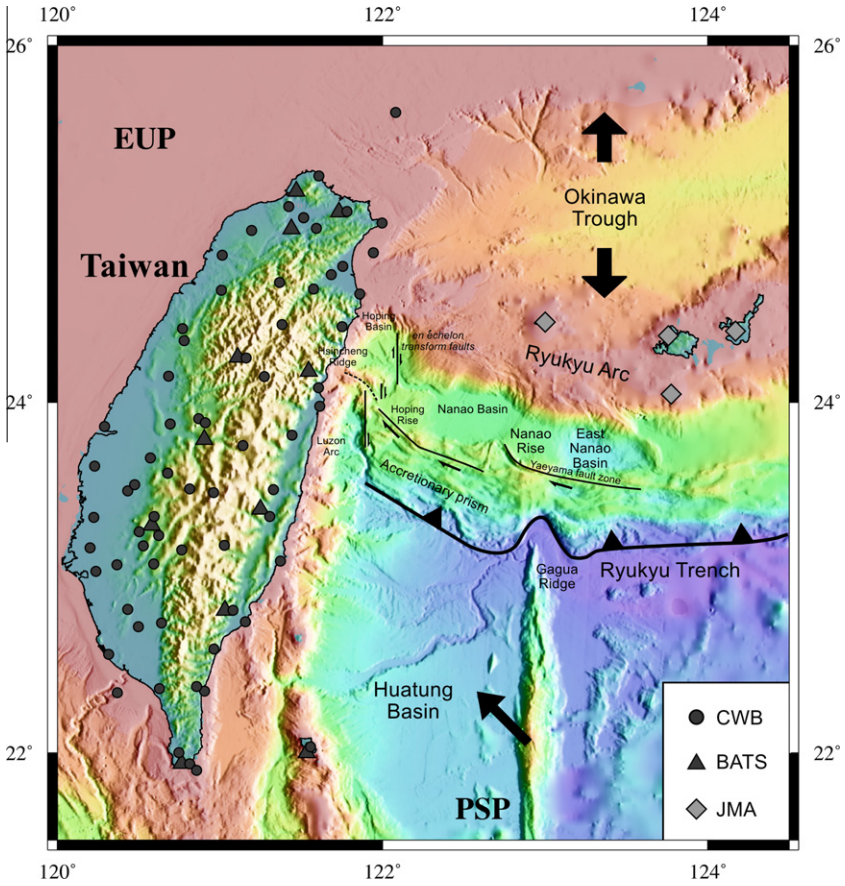

Fig. 1. Map of the southern Ryukyu subduction zone and station locations of permanent seismic networks that operate in the area (see text for more details). Thick black arrows show the direction of motion for the Philippine Sea plate (PSP) relative to the Eurasian plate (EUP) and the opening of the Okinawa Trough. Thin black lines represent faults and small arrows mark the relative motion between the two blocks. The position of the Ryukyu trench is shown with a thick black line marked with triangles (after Font et al., 2001).

and a transcurrent fault zone, called the Yaeyama Fault, formed as a result of the obliquity of the subduction. The largest sedimentary basins (Hoping, Nanao and East Nanao) are supplied with sediments produced by the erosion of the Taiwan mountain belt, through a system of numerous small canyons (Lallemand et al., 1997). A bathymetric high, known as the Nanao Rise, separates the Nanao and East Nanao basins and it is thought to be another manifestation of the subduction of the Gagua ridge (Schnurle et al., 1998; Font et al., 2001).

The seismotectonics of the southern Ryukyu subduction zone have been studied using focal mechanisms derived from modeling of teleseismic waveforms (Kao et al., 1998a) and from regional data recorded by permanent seismic stations in Taiwan (Kao et al., 1998b; Kao and Jian, 2001). These have been complemented with high-resolution earthquake locations obtained after combining phase arrivals picked at both Taiwanese and Japanese stations (Font, 2001; Font and Lallemand, 2009). Most of the seismicity exhibiting normal faulting is related either to the back arc extensional regime of the Okinawa Trough, or to the bending of the Philippine Sea plate in the outer Rise of the subduction zone. Pure and/or oblique thrust-type focal mechanisms prevail around the forearc sedimentary basins as a result of the fact that this area undergoes trench-perpendicular compression. Seismicity is also observed at the plate interface (20–30 km) and inside the subducting oceanic slab in the form of intermediate-depth earthquakes (70–300 km).

Several lines of evidence suggest that the Ryukyu plate interface near Taiwan is not strongly coupled (for an overview see Kao, 1998), therefore the generation of large (Mw >8) subduction earthquakes can be considered a very rare event. However, interactions among different tectonic stress regimes in the area (collision, oblique subduction, back arc extension) can cause the frequent occurrence of events with moment magnitudes between 6 and 7. Such earthquakes can still be hazardous for the nearby island of Taiwan and especially for its heavily populated cities like the capital Taipei which is built on a sedimentary basin. Recent strong-motion observations have shown that shallow earthquakes originating offshore the eastern coast of Taiwan produce high amplification within the Taipei basin at frequencies 0.3–1 Hz and are potentially dangerous for high-rise buildings and highway bridges (Sokolov et al., 2009). Despite the hazard posed, to-date there is no detailed information about the rupture process of any large offshore event in southern Ryukyus and its relation to regional seismotectonics. This is mainly due to the remoteness of the area that places it far from permanent seismic networks, as well as to the poorly constrained source-receiver velocity structure.

On 18 December 2001 at 04:03 (GMT) a powerful earthquake (Mw ~6.8) occurred near the Nanao basin and was strongly felt in Taipei and throughout Taiwan. This work takes advantage of both regional and teleseismic waveform data along with efficient location and source inversion techniques in order to elucidate the properties of this event. First, a brief description of its characteristics is given in terms of mainshock initial location and faulting mechanism information. Then both the mainshock and a large number of its aftershocks are accurately located using arrival times from all available stations and utilizing a 3D geo-realistic *a priori* velocity model. Then a finite fault representation of the mainshock

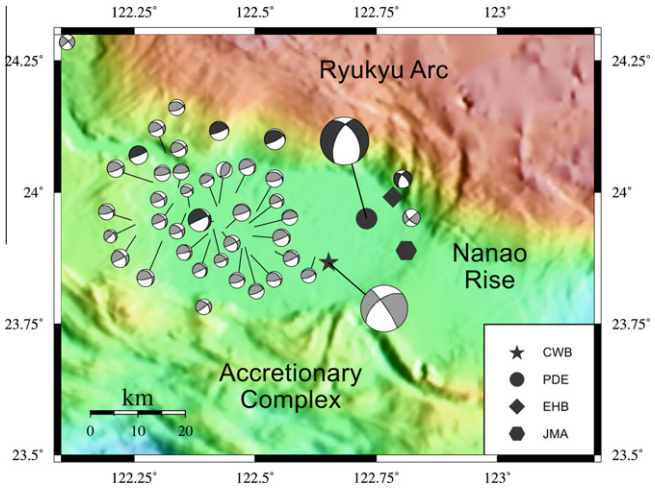

Fig. 2. Map of the area that covers the Nanao sedimentary basin and the uplifted area of the Nanao Rise. Black beach balls represent GCMT moment tensor solutions for moderate to strong shallow events that occurred prior to the 18 December 2001 earthquake. Gray beach balls represent BATS moment tensor solutions for smaller shallow events (Mw <4.5). Locations of the 18 December mainshock reported by different agencies are shown with different symbols. The large beach balls represent the revised GCMT (black) and BATS (gray) moment tensor solutions for the mainshock.

source process is derived using teleseismic waveform data. Finally, we close with a discussion of the rupture process and its relation to the tectonics of the area.

2. Mainshock characteristics

The mainshock was located by two regional agencies, Taiwan's Central Weather Bureau (CWB) and the Japanese Meteorological Agency (JMA), which both operate seismic networks near the focal area (cf. Fig. 1). Due to its large magnitude the event was also listed in the PDE catalog and in the updated global relocation database of Engdahl et al. (1998) (hereafter referred to as EHB). Fig. 2 shows a map of the broader focal area with these four different locations while Table 1 summarizes the available location information provided by the aforementioned agencies/catalogs. Even though all these locations seem quite consistent regarding the hypocentral depth of the mainshock (12–14 km), there is a difference in the epicentral estimates. Two of the epicenters (CWB and PDE) lie within the Nanao sedimentary basin, the EHB location is further north on the Ryukyu arc slope while the JMA epicenter is next to the Nanao Rise. Such a scatter can be considered reasonable if we take into account the large azimuthal gaps in station coverage that exist for an area like the southern Ryukyus.

Revised moment tensor solutions for the mainshock are provided by two groups, namely BATS (Broad-band Array in Taiwan for Seismology) and the Global CMT group (GCMT, former Harvard CMT). The BATS group routinely calculates moment tensor solutions for events in and around Taiwan since 1996 by inverting regional, three-component waveforms recorded by the BATS seismic network (Fig. 1 shows BATS deployment at the time of the earthquake). Their methodology utilizes different 1D velocity models for different stations and a variable inversion passband depending on event magnitude and background noise (for details see Kao et al., 1998b). The GCMT group inverts teleseismic waveforms by using three distinct wave types (body, surface and mantle waves for large events) also estimating centroid location and depth (e.g., Hjörleifsdottir and Ekström, 2010). The BATS solution gives for the mainshock a minimum misfit depth of 12 km and a focal mechanism exhibiting normal faulting with a substantial strike-slip component (Fig. 2). On the other hand, the GCMT solution also shows normal faulting accompanied by a smaller strike-slip contribution and a centroid depth of 16 km. Moment tensor solutions of past earthquakes in this area, either provided by GCMT (for Mw 5.1–6.0) or by BATS (for Mw <5), show in most cases low-angle thrust faulting inside the Nanao basin and only two of them located near the Ryukyu arc slope are compatible with the mainshock focal mechanism.

Table 1
Summary of source parameters for the 18 December 2001 earthquake reported in different catalogs. M_L is the local magnitude determined by CWB, M_j refers to the magnitude scale used by JMA, M_s is surface wave magnitude and Mw refers to moment magnitude derived by the GCMT group.

Catalog	Origin time	Latitude	Longitude	Depth (km)	Magnitude
CWB	04:03:0.75	23.867	122.652	12	6.7 (M_L)
JMA	04:02:59.39	23.8893	122.8120	12	7.3 (M_j)
PDE	04:02:58.30	23.950	122.730	14	7.3 (M_s)
EHB	04:02:59.69	23.991	122.785	14	6.8 (Mw)

3. Absolute earthquake locations

The 18 December event was followed by numerous smaller aftershocks that were recorded by the permanent seismic network stations in Taiwan and southern Ryukyu islands. The accurate location of this earthquake sequence hinges upon two main difficulties, namely station azimuthal coverage and the velocity model that will be used for travel time calculations. In this work, we deal with these problems by combining arrival times from both CWB and JMA networks, thus minimizing the azimuthal gap as much as possible and utilizing a three-dimensional velocity model derived for this area by Font et al. (2003). An improved version of the maximum intersection technique (MAXI) is utilized in order to obtain precise absolute locations of the mainshock and a large number of aftershocks. A description of the method and its application to the seismicity of the southern Ryukyus area can be found in Font et al. (2004) and Theunissen et al. (2009), therefore only a brief overview will be given here.

MAXI results from the modification of the master event method (Zhou, 1994) which locates each seismic event independently. First, the hypocenter is predetermined (PRED node) by finding the intersection point of all possible combinations of equal differential time (EDT) surfaces, so that in a network with j stations $j(j-1)/2$ EDT surfaces are constructed. An EDT surface is a deformed hyperbola defined by the collection of spatial points that satisfy the time difference between P-wave arrivals at a pair of stations. An EDT surface is independent of the earthquake origin time and includes the hypocenter. Subsequently, the MAXI search process does not suffer from the trade-off between the depth parameter and the origin time, and is therefore able to achieve a good approximation of depth using only P-arrivals and a 3D P-velocity model that well represent the structural complexity of the study area. An iterative process on the parameter that controls the EDT thickness allows a better survey of the solution domain. Second, a statistical analysis on the EDT intersection rate per seismic station is conducted to detect inconsistent arrivals from the initial dataset. Another main advantage of the MAXI algorithm is its ability to filter spurious measurements independently from the computation of travel-time residuals. Third, an iterative process of EDT intersections based on a cleaned set of arrival times is performed within a restricted volume resulting in a unique final solution. MAXI algorithm allows the determination of new confidence factors. The Qedt quality parameter indicates the percentage of EDT surfaces crossing through PRED with respect to the total number of EDT surfaces involved in the process. Qedt is independent

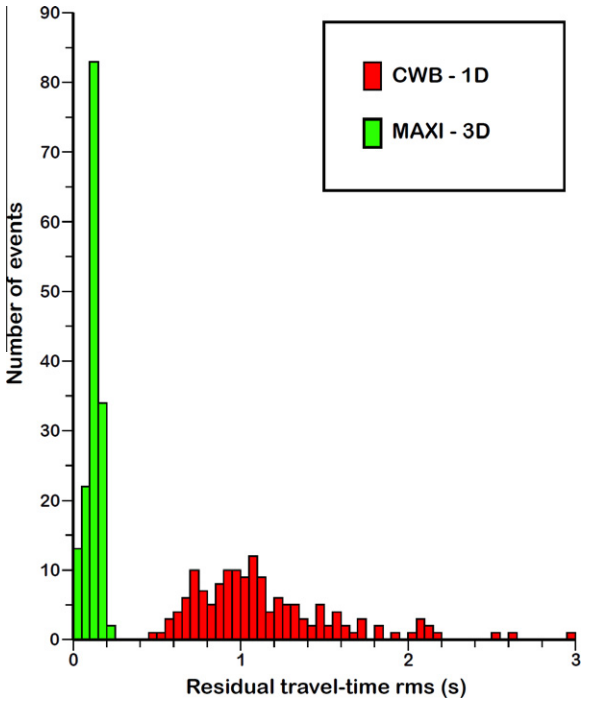

Fig. 3. Histogram showing the distribution of rms residuals for the aftershock locations determined with a 1D velocity model by CWB and with the 3D velocity model of Font et al. (2003) in this study. (For interpretation to colours in this figure, the reader is referred to the web version of this paper.)

from residual statistics and objectively quantifies the consistency between the arrival-time dataset, the velocity model used in the hypocenter determination process and MAXI procedure parameterization.

For the purpose of relocating the earthquake sequence of the 18 December event using the MAXI algorithm we combined the P-wave arrival times recorded at 38 CWB and 7 JMA stations (on average, the processed events included 15 ± 6 records). Most of the CWB stations correspond to locations in the eastern coast/NE of Taiwan while the JMA stations used are located at the Ryukyu islands of Yonaguni, Iriomote, Ishigaki and Hateruma covering an azimuth of approximately 270 degrees around the epicenter (see Fig. 1). From the initial dataset, we select the set of solutions whose Qedt is greater than 0.5. We evaluate the quality of this relocation by considering the reduction in the rms residual value after the relocation (Fig. 3). It can be seen that the rms residuals of CWB determinations are larger, having a mean value of 1.36 s (±1.50 s, median is 1.06) which after the relocation using MAXI within the 3D heterogeneous velocity model the rms mean value drops to 0.12 s (±0.04 s). The finally relocated catalog of events consists of the mainshock and 153 of its aftershocks. Estimation of uncertainties within MAXI follows the approach of Sambridge and Kennett (1986) that monitors the behavior of the residual statistics in the solution space. For our relocated events the average horizontal (x, y directions) and vertical uncertainty is 0.6–0.8 km and 1.6 km, respectively.

Fig. 4 shows a map of these relocated epicenters superimposed on the bathymetry of the study area along with two depth cross-sections. The mainshock is relocated at the edge of the Nanao basin (exact location 122.7758°E, 23.9328°N) very near the point where the Nanao Rise meets the Ryukyu arc slope. Its hypocentral depth is 9 km which agrees rather well with the depth of 12–14 km reported in the aforementioned catalogs (CWB, JMA, EHB, PDE) and signifies that the mainshock first affected the Ryukyu arc overriding basement. The rest of the aftershocks form several smaller clusters and most of them are located beneath the Ryukyu arc slope. The depth distribution of the hypocenters reveals that most of them occur between 5 and 15 km, a smaller part affecting the downgoing Philippine Sea plate or plate interface (below ~17 km depth). Based on the aftershock distribution and the available focal mechanism solutions it seems that the fault plane is the one following the NE–SW direction dipping to the NW. This suggestion will be further evaluated during the finite fault inversion described in the next section.

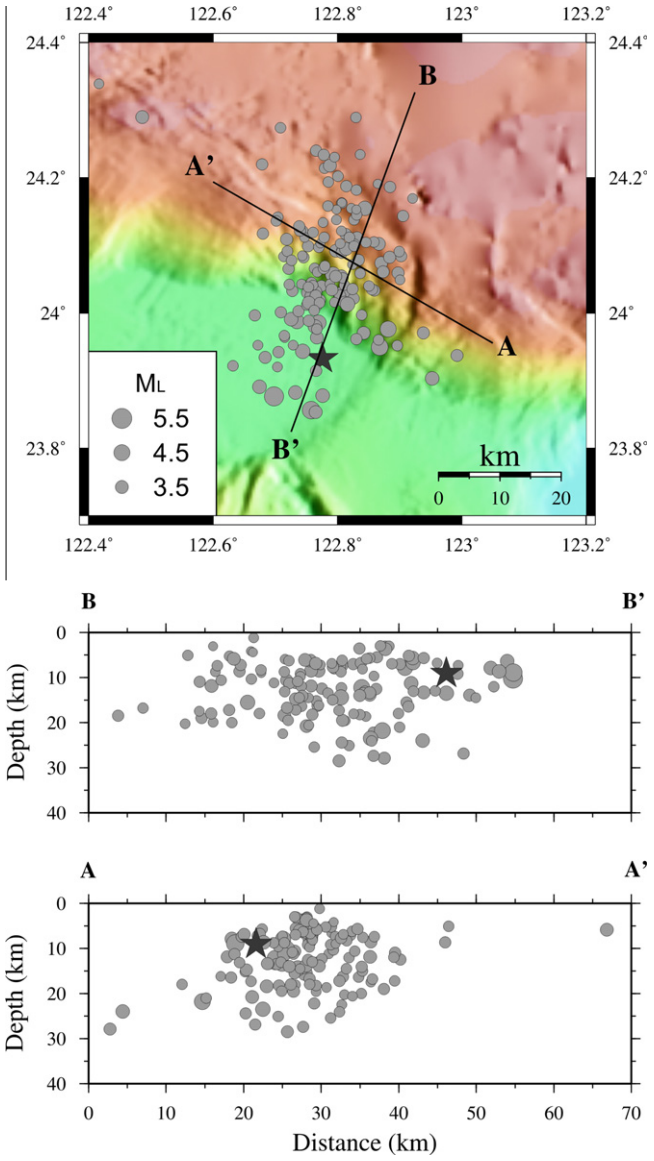

Fig. 4. Map of the earthquake locations (mainshock and 153 aftershocks) determined by using the MAXI technique and a 3D P-wave velocity model. The black star is the mainshock epicenter while the gray circles represent aftershock epicenters. The size of each circle is a function of the local magnitude estimated for each aftershock by CWB. The two black lines (AA′ and BB′) mark the direction of the two depth cross-sections shown at the bottom.

4. Finite fault inversion

4.1. Data and method

In this study, we invert teleseismic waveform data in order to derive the spatio-temporal pattern of slip distribution for the 18

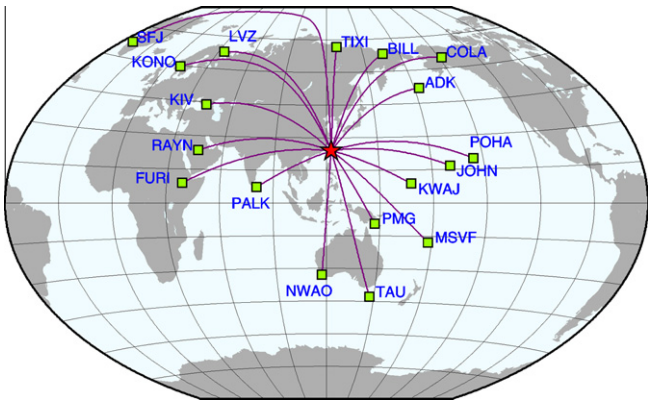

Fig. 5. Map of the globe showing the location of the mainshock (red star) and the locations of the 18 stations that were selected for the finite fault inversion. Purple curves represent Great Arc paths from source to receiver. (For interpretation of the references to color in this figure legend, the reader is referred to the web version of this paper.)

December main event. The reasoning behind the choice of using far- rather than near-field data lies on two factors: (a) stations at teleseismic distances are azimuthally distributed around the source thus minimizing inversion artifacts due to large station gaps, and (b) because of the propagation of seismic waves through geologically complex areas such as the trench and the Taiwan orogen, near-field records exhibit path effects that are difficult to match at higher frequencies using existing velocity models. We select stations based on their azimuth, waveform quality and epicentral distance which is limited to the range 30–100° in order to avoid complexities of Earth structure. These selection criteria yield 18 stations with good quality recordings of P and SH waveforms (Fig. 5). Once the data are obtained from the IRIS database the instrument response is removed, then waveforms are filtered between 0.01 and 0.5 Hz and are re-sampled using a sampling interval of five points per second.

The finite fault inversion problem is formulated as $\mathbf{Ax} = \mathbf{b}$ where $\mathbf{A}$ is the Green's function matrix, $\mathbf{b}$ is the observed data vector and $\mathbf{x}$ is the solution vector of slip on each subfault (e.g.,

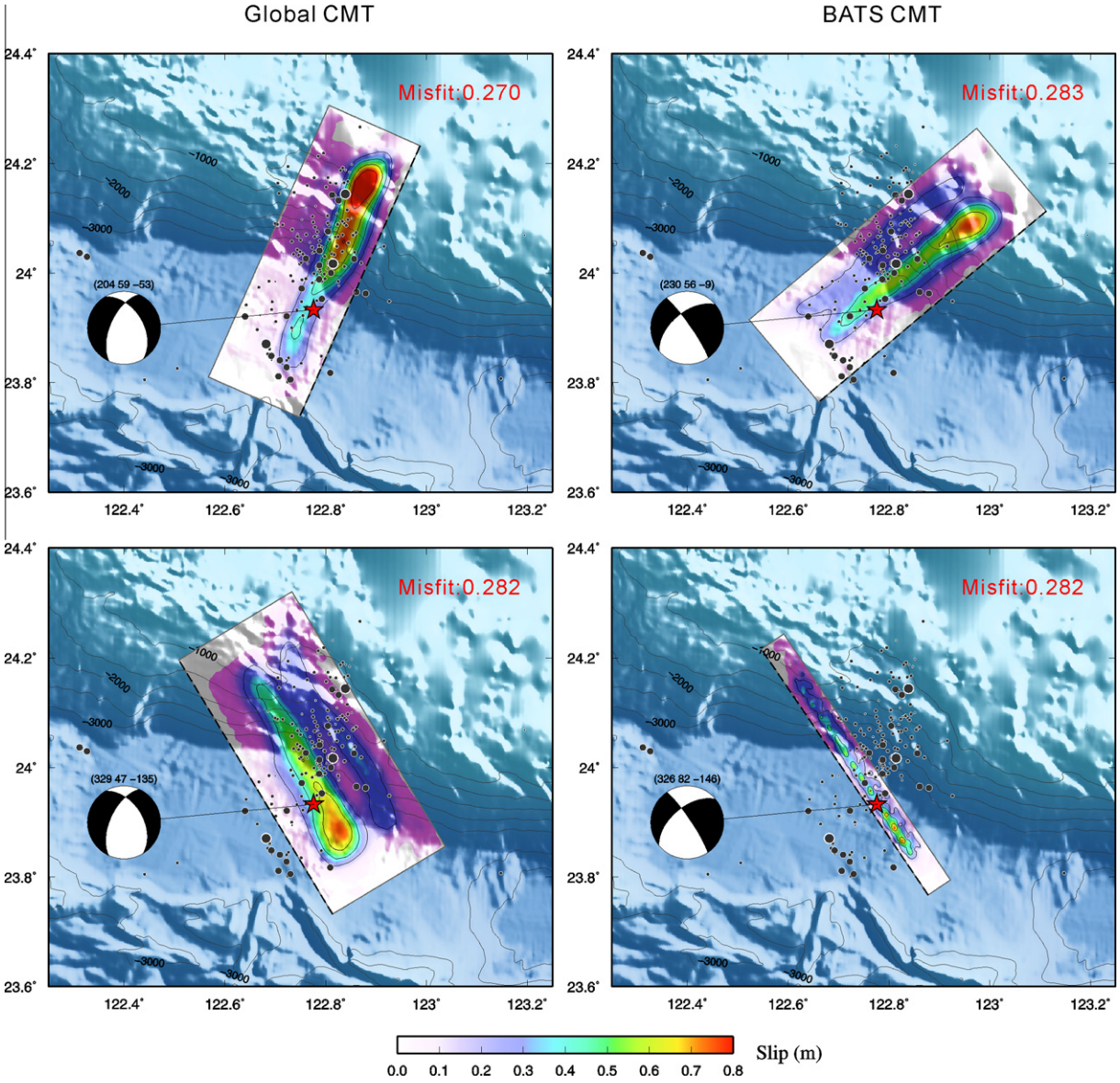

Fig. 6. Slip inversion results for the 18 December event for focal mechanism solutions and their nodal planes reported by the GCMT and BATS groups. Slip values vary according to the color scale shown at the bottom of the figure. The red star indicates the location of the mainshock and black circles the relocated aftershocks. On top of each beach ball are the strike, dip, rake value of each nodal plane that is tested in the inversion. (For interpretation of the references to color in this figure legend, the reader is referred to the web version of this paper.)

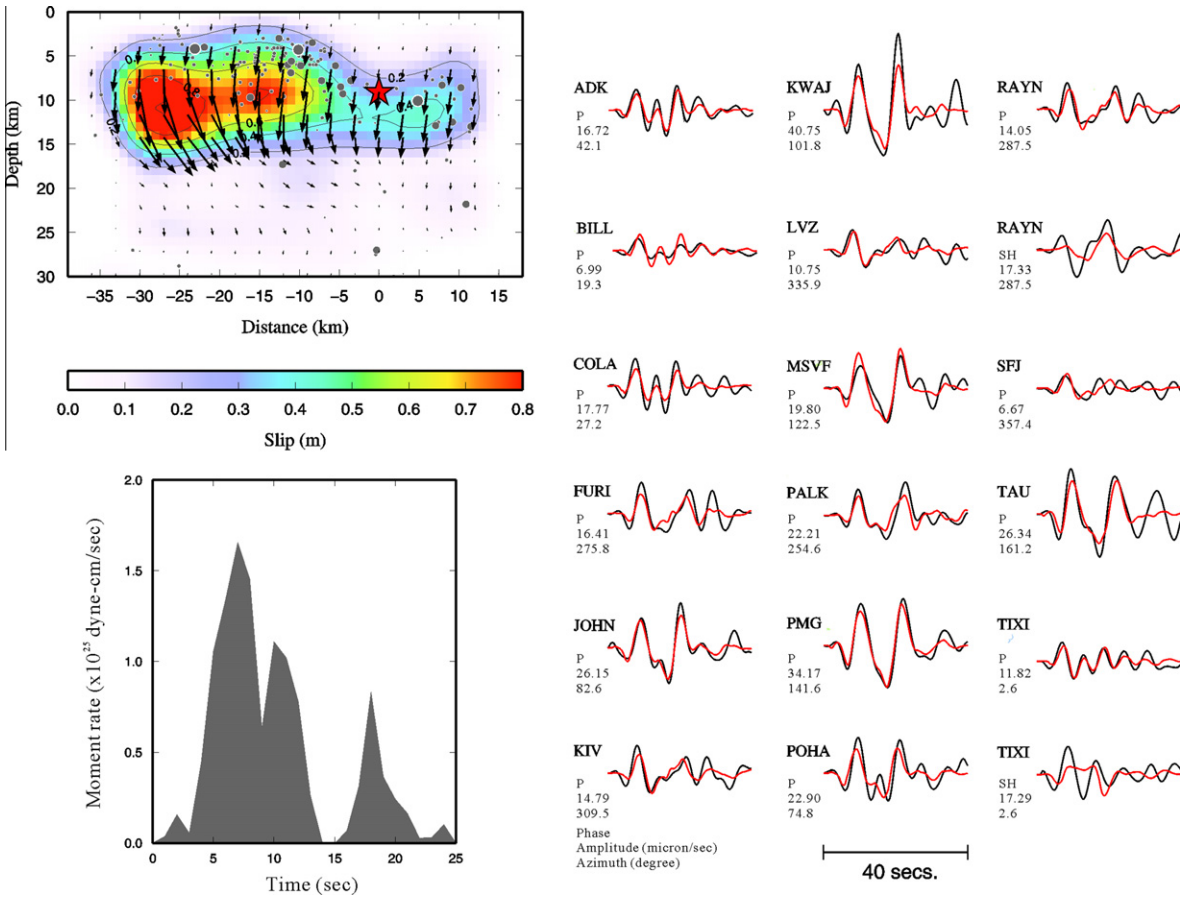

Fig. 7. Slip distribution (NE–SW direction) and observed (black curves) versus synthetic (red curves) waveforms of the preferred inversion solution. The estimated moment rate function can be seen at the lower left corner of the plot. All other symbols plotted are the same as previously. (For interpretation of the references to color in this figure legend, the reader is referred to the web version of this paper.)

Hartzell and Heaton, 1983). Lee et al. (2006) considered an improvement to this formulation by introducing multiple time windows along with parallel computing in an effort to obtain a better spatial and temporal resolution of slip. In this approach, matrix **A** is rearranged by taking Nt time windows and putting them side by side, while vector **x** becomes Nt times the single time window. Calculations are performed using a parallel non-negative least-squares (NNLS) inversion technique which decomposes matrix **A** into different computing nodes and solves for the vector **x** for each time window. We use a misfit function defined as $\mathbf{(Ax - b)^2/b^2}$ in order to evaluate the quality of a solution. Specific applications of this inversion algorithm to regional waveform data can be found in Lee et al. (2006) or Konstantinou et al. (2009a,b). Teleseismic Green's functions are calculated by using the method of Kikuchi and Kanamori (1982) utilizing the 1D PREM model (Dziewonski and Anderson, 1981). Once Green's functions are computed they are filtered between 0.01 and 0.5 Hz in the same way as the data.

4.2. Preferred solution and sensitivity tests

The first step towards developing a slip distribution model for the 18 December main event involves deciphering which of the two revised moment tensor solutions (GCMT, BATS) and nodal planes fit the data better. We applied the finite fault inversion algorithm described earlier using 24 time windows and a fault plane that consists of individual subfaults with dimensions 3×3 km. The total area covered by the fault plane has a length of 55 km and down-dip width of 30 km, values that have been chosen so as to avoid any underestimation of the true fault plane. Each subfault is allowed to slip in any of the 2 s time windows following the passage of the rupture front while each time window has an overlap of 1 s. Thus each subfault can slip within any time period of 25 s after the rupture front has passed through. We also assume a value of rupture velocity in order to initiate the calculations, however, this parameter is allowed to vary during the inversion process.

After running a set of inversions assuming different focal mechanisms and considering both nodal planes, we find that the GCMT solution and the nodal plane trending NE–SW exhibit the lowest misfit (Fig. 6). The difference in misfit between this and the other slip distributions is not great and therefore we use the relocated aftershocks pattern as primary constraint in order to decide in favor of the aforementioned focal mechanism and nodal plane. Fig. 7 shows a depth cross-section view of this preferred slip distribution with the relocated aftershocks superimposed and also the corresponding waveform fits along with the moment released as a function of time. However, the inability to discriminate between fault and auxiliary plane is often considered as an indication of a point rather than an extended source. In order to check whether a simpler source model can also explain the observed waveforms we assumed a slip distribution that resembles a small symmetrical patch encircling the hypocenter (Fig. 8). Based on this slip model synthetic seismograms are calculated for the 18 stations using again the PREM model. The comparison of these synthetics with the observed waveforms

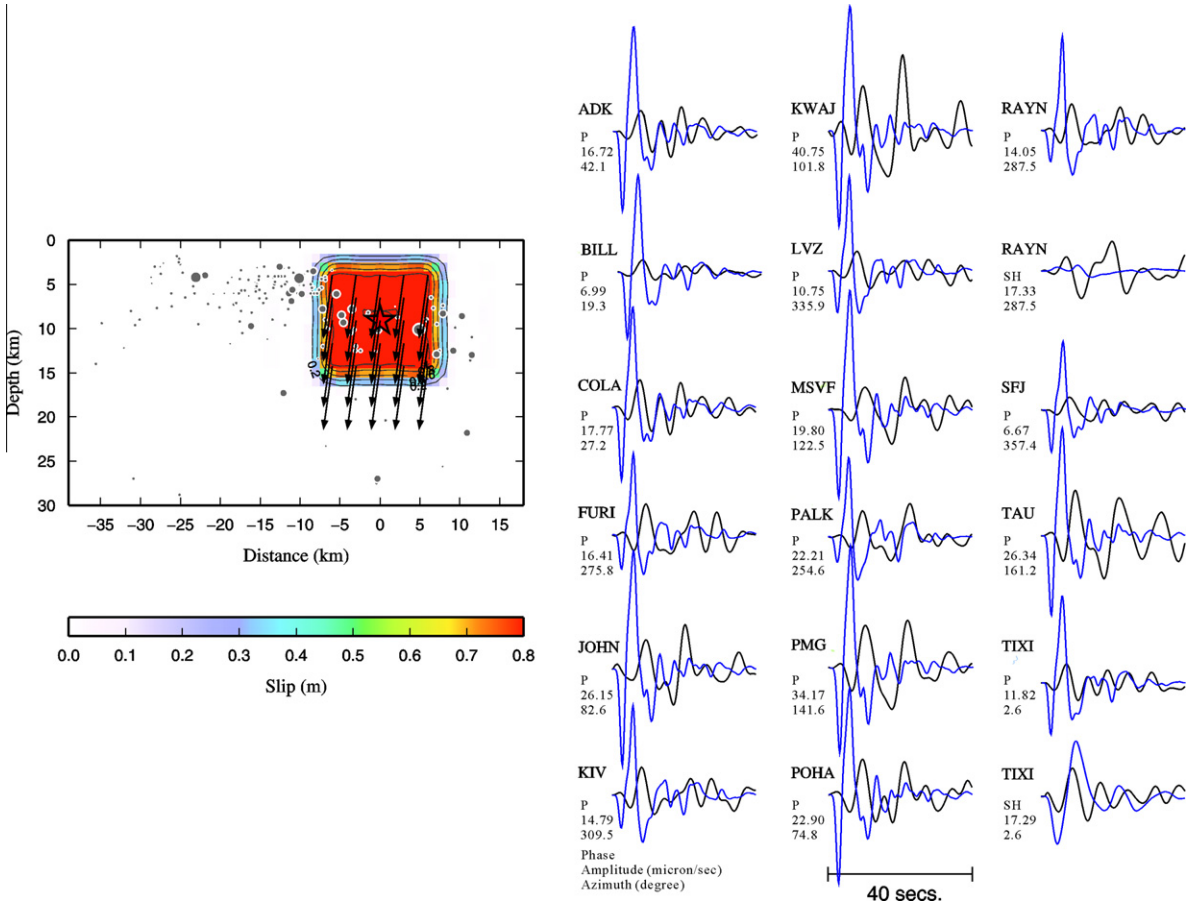

Fig. 8. Test that considers whether the source of the 18 December mainshock can be approximated by a smaller symmetric patch shown in the left hand side of the plot. Aftershocks locations are shown as black dots for reference while the star represents the hypocenter of the mainshock. Black curves signify the observed waveforms and blue ones the synthetics. All other symbols plotted are the same as previously.

reveals a much worse fit than the one obtained previously from the finite fault modeling (see Fig. 7), even though in some individual stations (e.g., TIXI) the fit is acceptable for the later part of the seismogram. We conclude therefore that such a simple, small-size source cannot adequately explain the observed waveform features at most of the stations.

For the purpose of assessing the uncertainties of our preferred slip distribution model we conducted a series of tests by varying the inversion parameters and model settings. First, we performed a resolution test where we assumed a slip distribution consisting of three patches of different size (smallest patch is 12×9 km) and slip amplitude (Fig. 9). Using this model we calculated synthetic seismograms for each of the 18 stations which were subsequently inverted in order to recover the slip distribution using the same parameters as above and assuming three different subfault dimensions (2×2, 3×3, 4×4 km). It can be seen that in the 2×2 and 3×3 km cases the slip pattern can be almost fully recovered both for the high ($\sim$0.9 m) and the low ($\sim$0.2 m) amplitude slip patch. There are only some minor distortions of the patches from the original square shape and some overestimation of the slip amplitude for some of the patches. As the subfault size increases to 4×4 km the resolution starts deteriorating significantly leading to a pattern of interconnected patches which does not represent the input model.

The next test evaluates the influence that selected stations may have on the preferred solution either from the viewpoint of azimuth/distance or particular propagation path. Towards this end, we performed another set of inversions excluding one station at a time and afterward taking the average of the resulting slip distributions (Fig. 10). It is expected that this averaging will smooth any artifacts introduced by any particular station and sharpen the features that are common in all solutions. The results of this test reveal that the preferred slip model is quite stable with respect to different combinations of stations being used in the inversion. Exclusion of stations KIV, PALK, PMG and LVZ seems to result in the creation of two separate rather than one big asperity, however, this is not seen in the other trial inversions nor the average solution. Finally, we try to determine the optimum number of multiple-time windows that should be used in order to resolve the slip distribution in both time and space. A set of inversions with multiple-time windows in the range 4–24 were carried out and the results can be viewed in Fig. 11. It is evident that 20–24 time windows are needed in order to sufficiently minimize the misfit and resolve both the temporal and spatial slip pattern. An increase in the number of time windows beyond this value apparently does not result in any significant improvement of the solution.

5. Discussion

5.1. Rupture process of the mainshock

In the preferred slip distribution model the largest patch, that also exhibits the highest slip amplitude ($\sim$0.8 m), extends from 5 km to about 16 km depth and appears elongated in the

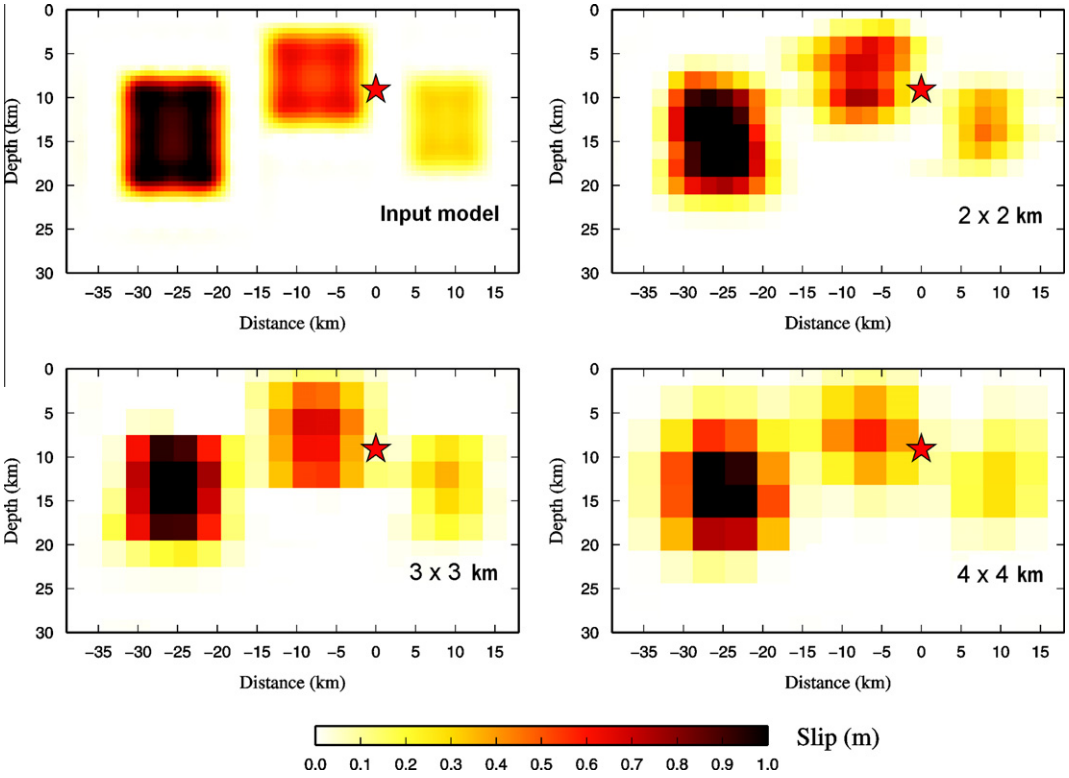

Fig. 9. Resolution test performed assuming the slip distribution model shown at the top left map. Results are presented as a function of subfault dimensions (see text for more details). The star represents the hypothetical hypocenter of the mainshock. All other symbols plotted are the same as previously.

NE–SW direction. A smaller patch exists at the one end of the fault plane at depths between 10 and 15 km exhibiting a slip amplitude that is not higher than about 0.4 m. The relocated hypocenter of the main event falls in the area between these two patches indicating that the rupture was probably bilateral. Most aftershock hypocenters are located in the periphery of the largest patch while relatively few of them appear close to the smaller one (where the overriding basement is also much thinner). Such a distribution agrees well with numerous observations stating that aftershocks following large earthquakes usually coincide with areas of low slip (in this case smaller than 0.5 m) therefore they originate at regions of slip deficit. It is quite interesting to note that the upper edge of slip distribution seems to follow the seafloor topography with only a minor slip patch contained inside the Nanao basin. This can be explained by considering that the rupture propagated efficiently through the crystalline arc basement but not through the soft material covering the basin. The lower edge of the slip distribution also seems to follow the interplate contact zone, when referring to images from seismic refraction experiments (McIntosh and Nakamura, 1998; Wang and Chiang, 1998; Wang and Pan, 2001).

The temporal variation of seismic moment that was released during the fault rupture has a total duration of 25 s and exhibits a number of discrete peaks. The largest peak occurs after about 6 s implying a delayed rupture of the main asperity. In order to obtain a better perspective of the source process, we create a series of snapshots that show how the slip distribution evolved through space and time (Fig. 12). During the first 4 s small patches of slip appear in the NE direction, corresponding to the small initial peak that can be seen in the moment rate function. At around 6 s a larger amount of slip starts initiating in the same area northwards from the hypocenter. Between 8 and 12 s the large slip patch is finally formed, while the time of its formation coincides with the two largest peaks of moment release. At later times (14–20 s) the amount and extent of the large patch does not change much, however, the smaller patch is formed to the SW of the hypocenter. After this time the slip distribution pattern changes very little and the amount of moment that is released also drops significantly.

5.2. Seismotectonic implications

The location of the 18 December main event obtained with the MAXI algorithm is placed close to the area where the Nanao Rise meets the Ryukyu arc slope. Aftershock locations and the results of the finite fault inversion show that it was caused by a westward dipping fault trending NE–SW and extending from the edge of the Nanao Rise to the Ryukyu arc basement. This particular area has been studied in detail by Schnurle et al. (1998) and Font et al. (2001) using accurate seafloor topographic and seismic reflection data. The authors found that the Nanao Rise is bounded to its eastern and western edges by sets of normal faults. The faults at the western edge dip westwards and cut through the forearc crystalline basement and the deposited sediments in the Nanao basin. The offsets of these faults and the divergent depositional character of the sediments suggest that the forearc basement of the Nanao Rise is steadily uplifting since at least 1 Ma (Dominguez et al., 1998). Such an observation implies that the uplift of the Nanao Rise is syn-sedimentary and that faulting is still active, a conclusion that is also in agreement with the findings of this work.

It has long been suggested that the forearc basement uplift which has generated the Nanao Rise is the result of the subduction of a Gagua ridge segment (Schnurle et al., 1998; Dominguez et al., 1998; Font et al., 2001; Wang and Pan, 2001; Wang et al.,

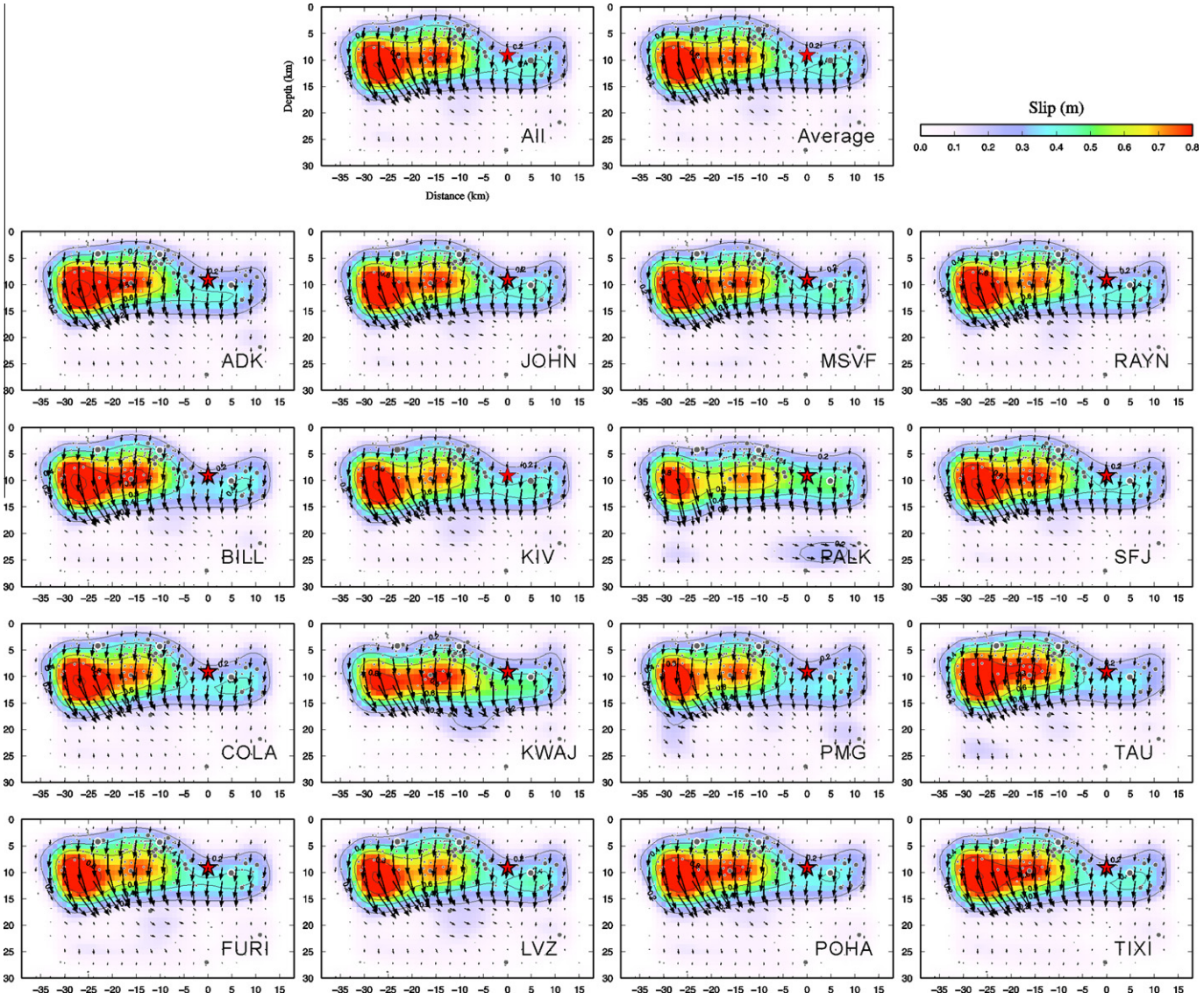

Fig. 10. Station combination test. Separate inversions are performed each time excluding data from one station. The resulting slip distribution can be seen in each case. The average slip distribution from all these inversions is shown on top along with the slip distribution using all stations. Black arrows indicate the sense of slip motion on the surface of the fault. All other symbols plotted are the same as previously.

2004). This suggestion is supported by seafloor topography observations and analog sandbox experiments that show that an oblique ridge subduction is associated with deformation patterns consistent with those observed at the Ryukyu accretionary complex. A reconstruction of the Gagua ridge subduction after taking into account plate convergence rates indicates that over the last 1 Ma one segment of the ridge should already have been consumed. The toe of this segment may presently be located very near the Ryukyu arc slope and also near the epicenter of the 18 December earthquake (Fig. 13a). Subducting seamounts and fracture ridges have been known to withstand subduction forces due to the buoyant nature of their highly fractured material (Scholz and Small, 1997). This has been used as an argument to suggest that such subducted features may act as asperities, representing sites of future large earthquakes, even though there is also evidence that they may act as barriers to seismogenic ruptures (Kodaira et al., 2000).

Baba et al. (2001) have considered how a seamount or fracture ridge may deform during subduction by using finite element numerical simulations. The authors assume that the seamount has retained its original shape after subducting at shallow depth beneath the accretionary prism. This assumption is supported by the observation that subducted seamounts do not loose their magnetization thus their original shape is preserved (Barckhausen et al., 1998). The model predicts that at the seaward flank of the seamount the maximum principal stress due to the plate convergence will be almost horizontally oriented, while the minimum principal stress due to the reduced overburden will be vertical (Fig. 13b). This configuration favors the faulting of the subducted seamount and the creation of a seismogenic thrust fault as has been actually observed, for example in the case of the 1994 Java (Mw 7.6) earthquake (Abercrombie et al., 2001). In the landward flank of the seamount however, the overburden is thicker and the maximum principal stress is expected to be vertical with the minimum stress being horizontal. If the overburden is represented by low-cohesion sedimentary material commonly found in an accretionary complex, no seismogenic faulting will occur to the seamount and deviatoric stress will be released through inelastic deformation of the overlying sediments.

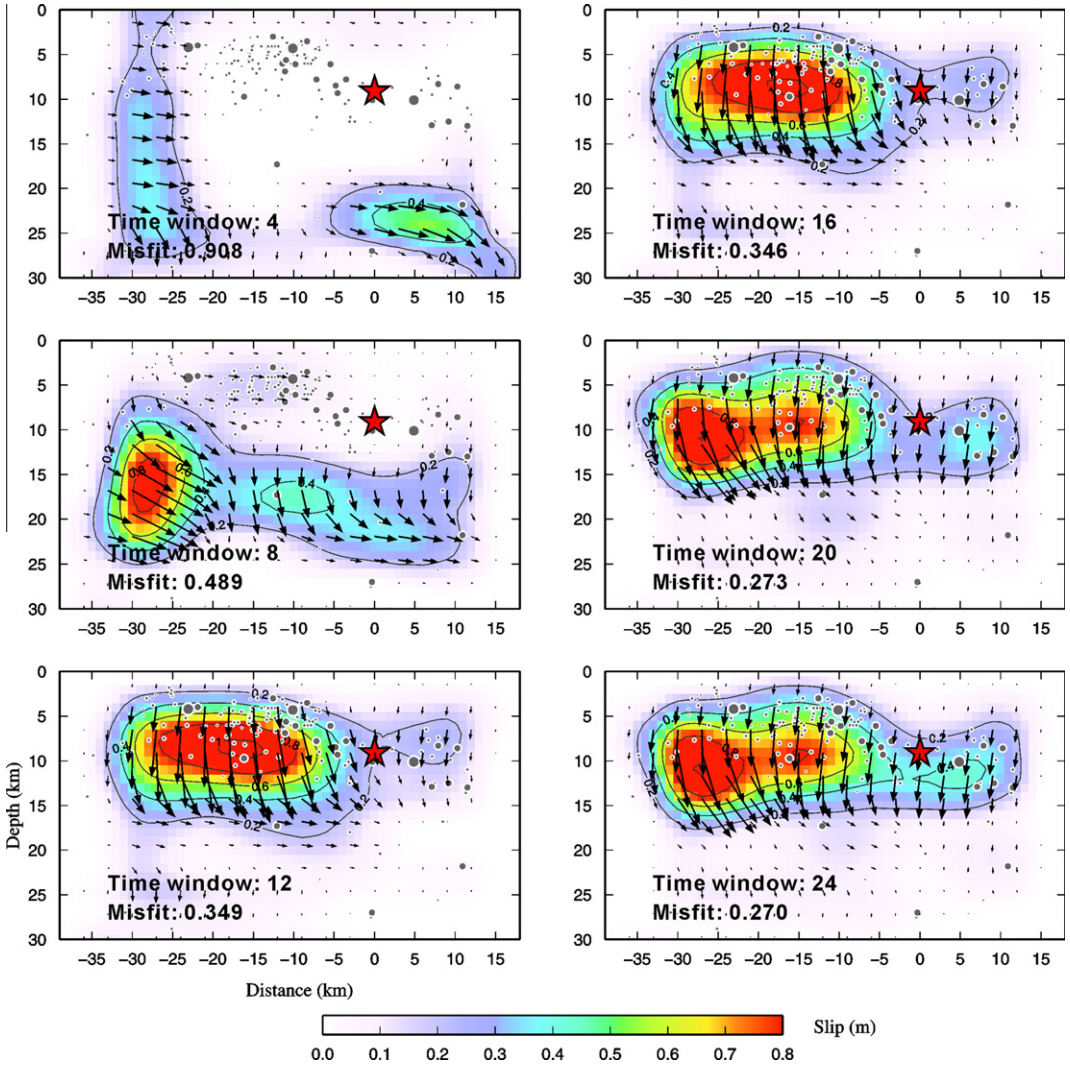

Fig. 11. Slip distribution stemming from inversions using a different number of time windows along with the corresponding misfit in each case. All other symbols plotted are the same as previously.

Such a model could be used in order to understand how the stress field generated by the subducted segment of the Gagua ridge might have influenced the nucleation of the 18 December event. However, two additional factors should be taken into account: first, that the subduction of the ridge is oblique in a direction close to N345°E (Dominguez et al., 1998) and second that in the front part of the subducted segment the material of the overburden consists of crystalline rocks of the Ryukyu arc basement, thus brittle instead of inelastic deformation is expected. The former factor implies that the orientation of the minimum stress should also be close to N345°E; the latter factor suggests that a vertical maximum stress should act at the basement rocks near the nucleation point of the mainshock as a result of the buoyancy of the Gagua ridge (Fig. 13c). This configuration of stresses is expected to generate normal faulting with some strike-slip component which is consistent with the faulting mechanism of the 18 December mainshock. Recently, Wu et al. (2010) inverted a large number of moment tensor solutions in order to infer the stress tensor along a regular grid of points covering the Ryukyu–Taiwan–Luzon area. Their results for the area around the Nanao Rise agree well with our interpretation described above, showing a minimum principal stress trending NW and a subvertical maximum principal stress.

6. Conclusions

The main conclusions of this work can be summarized as follows:

1. A precise absolute location using available arrival times from Taiwanese and Japanese stations and 3D geo-realistic *a priori* velocity model places the 18 December 2001 main event at the edge of the Nanao Rise, close to the Ryukyu arc slope. The shallow depth of the event (12–14 km) given by published locations and moment tensor solutions is confirmed by our hypocentral estimate of 9 km. The locations of the aftershocks delineate a NE–SW oriented fault which coincides with faults imaged in this area in seismic cross-sections published previously.
2. The preferred slip distribution model for the mainshock consists of one large slip patch with 0.8 m maximum amplitude extending through the Ryukyu arc basement. A much smaller patch with 0.4 m maximum amplitude exists at the side of the Nanao basin. Most of the slip is concentrated at depths 5–15 km while the upper edge of the slip tends to follow the seafloor topography. The located aftershocks are mostly clustered in the areas of slip deficit (<0.4 m).

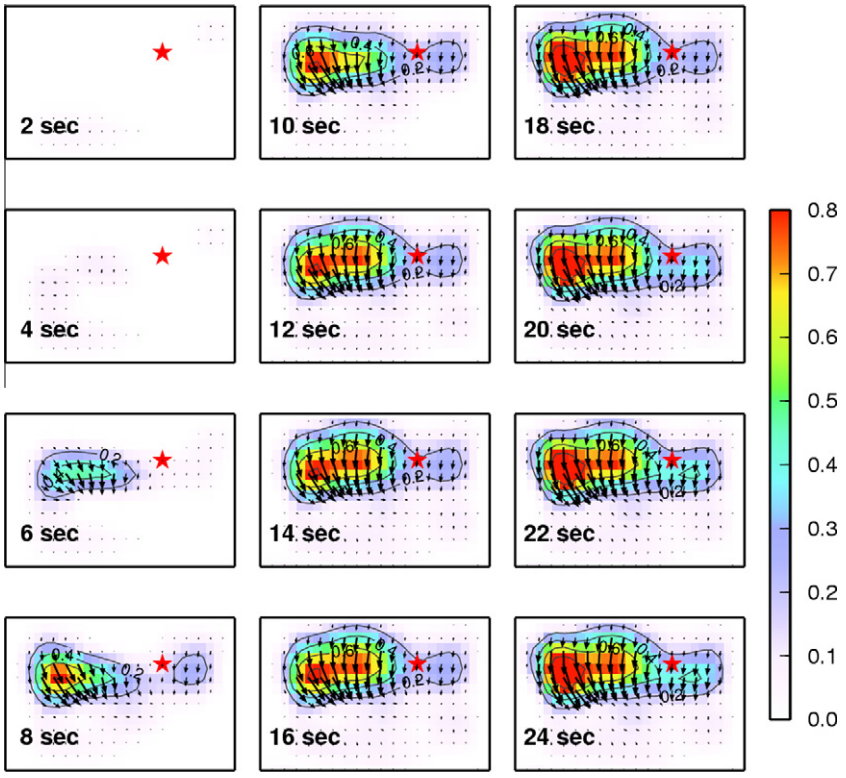

Fig. 12. Snapshots of the rupture process of the 18 December 2001 event depicted every 2 s. All other symbols plotted are the same as previously.

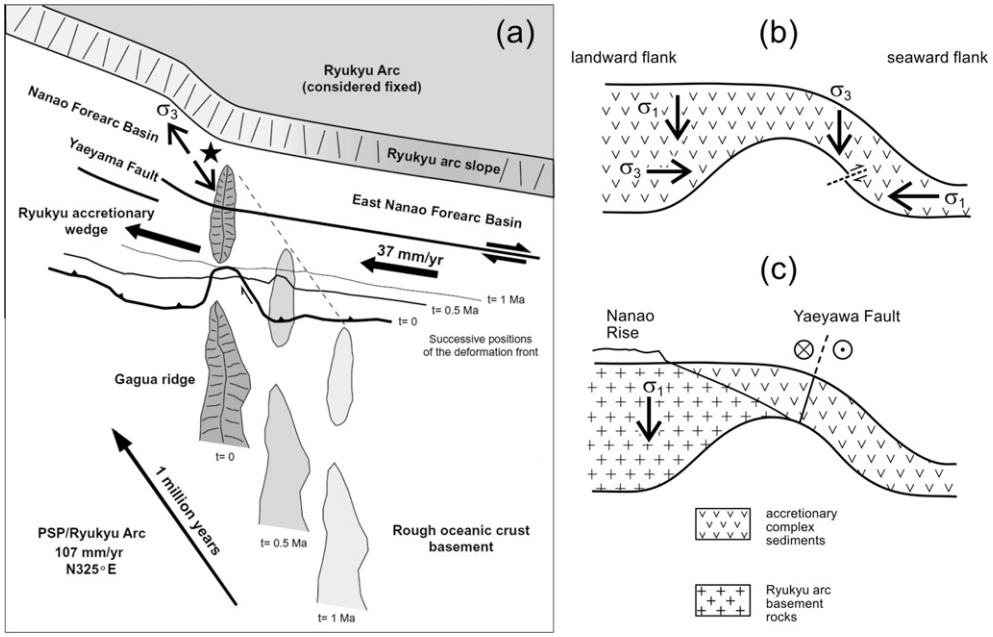

Fig. 13. (a) Reconstruction of the Gagua ridge subduction over the last 1 Ma based on the westward motion of the accretionary wedge at a rate of 3.7 cm year^{-1} (after Dominguez et al., 1998). The star represents the approximate location of the 18 December earthquake and the double arrow shows the direction of the minimum principal stress in the area which follows the obliquity of the subduction (see text for more details), (b) principal stress axes configuration at the seaward and landward flank of a subducting seamount or fracture ridge (after Baba et al., 2001). The seamount is assumed to subduct in a direction perpendicular to the trench. In this case it is expected that the seamount will fracture in its seaward flank and the landward sediments will be deformed inelastically, (c) possible configuration of the obliquely subducting Gagua ridge segment (sketch is not to scale). Its landward flank has impacted the Ryukyu arc crystalline basement where the maximum principal stress axis is vertical and brittle deformation is expected.

3. It is likely that the 18 December 2001 earthquake was caused by a stress field interaction generated by the oblique subduction of the Gagua ridge and the gravitational forces acting at its landward flank. These results are in agreement with previous assessments which state that such interactions are capable of causing strong earthquakes that can be hazardous for the nearby populated island of Taiwan.

Acknowledgments

K.I.K. and S.J.L. thank the National Science Council of Taiwan for the financial support of this research. The authors also thank the Editor George Helffrich and two anonymous reviewers for their helpful comments.

References

Abercrombie, R.E., Antolik, M., Felzer, K., Ekström, G., 2001. The 1994 Java tsunami earthquake: slip over a subducting seamount. J. Geophys. Res. 106, 6595–6607.

Baba, T., Hori, T., Hirano, S., Cummings, P.R., Park, J.-O., Kameyama, M., Kaneda, Y., 2001. Deformation of a seamount subducting beneath an accretionary prism: constraints from numerical simulation. Geophys. Res. Lett. 28, 1827–1830.

Barckhausen, U., Roeser, H.A., von Huene, R., 1998. Magnetic signature of upper plate structures and subducting seamounts at the convergent margin off Costa Rica. J. Geophys. Res. 103, 7079–7093.

Deschamps, A., Lallemand, S.E., Collot, J.-Y., 1998. A detailed study of the Gagua Ridge: a fracture zone uplifted during a plate re-organization in the Mid-Eocene. Mar. Geophys. Res. 20, 403–423.

Dominguez, S., Lallemand, S., Malavieille, J., Schnurle, P., 1998. Oblique subduction of the Gagua Ridge beneath the Ryukyu accretionary wedge system: insights from marine observations and sandbox experiments. Mar. Geophys. Res. 20, 383–402.

Dziewonski, A.M., Anderson, D.L., 1981. Preliminary reference Earth model. Phys. Earth Planet. Interiors 25, 297–356.

Engdahl, E.R., van der Hilst, R.D., Buland, R.P., 1998. Global teleseismic earthquake relocation with improved travel time and procedures for depth determination. Bull. Seismol. Soc. Am. 88, 722–743.

Font, Y., 2001. Modes of the ongoing arc-continent collisional processes in Taiwan: new insights from seismic reflection analysis and earthquake relocation, PhD thesis, National Taiwan University, 262 pp.

Font, Y., Liu, C.-S., Schnurle, P., Lallemand, S., 2001. Constraints on backstop geometry of the southwest Ryukyu subduction based on reflection seismic data. Tectonophysics 333, 135–158.

Font, Y., Kao, H., Liu, C.-S., Chiao, L.-Y., 2003. A comprehensive 3D seismic velocity model for the eastern Taiwan–southernmost Ryukyu regions. TAO 14, 159–182.

Font, Y., Kao, H., Lallemand, S., Liu, C.-S., Chiao, L.-Y., 2004. Hypocenter determination offshore of eastern Taiwan using the Maximum Intersection method. Geophys. J. Int. 158, 665–675. doi:10.1111/j.1365-246X.2004.02317.

Font, Y., Lallemand, S., 2009. Subducting oceanic high causes compressional faulting in southernmost Ryukyu forearc as revealed by hypocentral determinations of earthquakes and reflection/refraction seismic data. Tectonophysics 466, 255–267. doi:10.1016/j.tecto.2007.11.018.

Hartzell, S.H., Heaton, T.H., 1983. Inversion of strong ground motion and teleseismic waveform data for the fault rupture history of the 1979 Imperial Valley, California earthquake. Bull. Seismol. Soc. Am. 73, 1553–1583.

Hjörleifsdottir, V., Ekström, G., 2010. Effects of three-dimensional Earth structure on CMT earthquake parameters. Phys. Earth Planet. Interiors 179, 178–190. doi:10.1016/j.pepi.2009.11.003.

Kao, H., 1998. Can great earthquakes occur in the southernmost Ryukyu arc–Taiwan region? TAO 9, 487–508.

Kao, H., Shen, S.J.S., Ma, K.F., 1998a. Transition from oblique subduction to collision: earthquakes in the southernmost Ryukyu arc–Taiwan region. J. Geophys. Res. 103, 7211–7229.

Kao, H., Jian, P.-R., Ma, K.-F., Huang, B.-S., Liu, C., 1998b. Moment tensor inversion for offshore earthquakes east of Taiwan and their implications for regional collision. Geophys. Res. Lett. 25, 3619–3622.

Kao, H., Jian, P.-R., 2001. Seismogenic patterns in the Taiwan region: insights from source parameter inversion of BATS data. Tectonophysics 333, 179–198.

Kubo, A., Fukuyama, E., 2003. Stress field along the Ryukyu arc and the Okinawa Trough inferred from moment tensors of shallow earthquakes. Earth Planet. Sci. Lett. 210, 305–316, doi:10.1016/S0012-821X(03)00132-8.

Kodaira, S., Takahashi, N., Nakanishi, A., Miura, S., Kaneda, Y., 2000. Subducted seamount imaged in the rupture zone of the 1946 Nankaido earthquake. Science 289, 104–106.

Kikuchi, M., Kanamori, H., 1982. Inversion of complex body waves. Bull. Seismol. Soc. Am. 72, 491–506.

Konstantinou, K.I., Melis, N.S., Lee, S.-J., Evangelidis, C.P., Boukouras, K., 2009a. Rupture process and aftershocks relocation of the 8 June 2008 Mw 6.4 NW Peloponnese, Western Greece. Bull. Seismol. Soc. Am. 99, 3374–3389. doi:10.1785/0120080301.

Konstantinou, K.I., Lee, S.-J., Evangelidis, C.P., Melis, N.S., 2009b. Source process and tectonic implications of the 8 January 2006 (Mw 6.7) Kythira earthquake, southern Greece. Phys. Earth Planet. Interiors 175, 167–182. doi:10.1016/j.pepi.2009.03.010.

Lallemand, S.E., Liu, C.-S., Font, Y., 1997. A tear fault boundary between the Taiwan orogen and the Ryukyu subduction zone. Tectonophysics 274, 171–190.

Lee, S.-J., Ma, K.-F., Chen, H.-W., 2006. Three-dimensional dense strong motion waveform inversion for the rupture process of the 1999 Chi-Chi Taiwan, earthquake. J. Geophys. Res. 111, B11308. doi:10.1029/2005JB004097.

McIntosh, K., Nakamura, Y., 1998. Crustal structure beneath the Nanao forearc basin from TAICRUST MCS/OBS Line 14. TAO 9, 345–362.

Nakamura, M., 2004. Crustal deformation in the central and southern Ryukyu arc estimated from GPS data. Earth Planet. Sci. Lett. 217, 389–398, doi:10.1016/S0012-821X(03)00604-6.

Sambridge, M.S., Kennett, B.L.N., 1986. A novel method of hypocenter location. Geophys. J.R. Astron. Soc. 87 (2), 679–697.

Schnurle, P., Liu, C.-S., Lallemand, S.E., Reed, D.L., 1998. Structural insight into the south Ryukyu margin: effects of the subducting Gagua Ridge. Tectonophysics 288, 237–250.

Scholz, C.H., Small, C., 1997. The effect of seamount subduction on seismic coupling. Geology 25, 487–490.

Sokolov, V., Wen, K.-L., Miksat, J., Wenzel, F., Chen, C.-T., 2009. Analysis of Taipei basin response for earthquakes of various depths and locations using empirical data. TAO 20, 687–702. doi:10.3319/TAO.2008.10.15.01(T).

Theunissen T., Font Y., Gautier S., Lallemand S., Liang W.-T., 2009. 3D absolute earthquake location in subduction zone using MAXI method: application to the Ryukyu Subduction (Taiwan), T41B-2020, AGU Fall Meeting.

Tsai, Y.B., 1986. Seismotectonics of Taiwan. Tectonophysics 125, 17–38.

Wang, T.-K., Chiang, C.-H., 1998. Imaging of arc-arc collision in the Ryukyu forearc region offshore Hualien from TAICRUST OBS line 16. TAO 9, 329–344.

Wang, T.K., Pan, C.H., 2001. Crustal Poisson ratio off eastern Taiwan from OBS data modeling, TAO, suppl. Issue, 249–268.

Wang, T.K., Lin, S.-F., Liu, C.-S., Wang, C.-S., 2004. Crustal structure of the southernmost Ryukyu subduction zone: OBS, MCS and gravity modeling. Geophys. J. Int. 157, 147–163.

Wu, W.-N., Kao, H., Hsu, S.-K., Lo, C.-L., Chen, H.-W., 2010. Spatial distribution of the crustal stress field along the Ryukyu–Taiwan–Luzon convergent boundary. J. Geophys. Res. 115, B11401. doi:10.1029/2009JB007080.

Wu, F.T., Rau, R.J., Salzberg, D., 1997. Taiwan orogeny: thin-skinned or lithospheric collision? Tectonophysics 274, 191–220.

Yeh, Y.H., Barrier, E., Lin, C.H., Angelier, J., 1991. Stress tensor analysis in the Taiwan area from focal mechanisms of earthquakes. Tectonophysics 200, 267–280.

Yu, S.-B., Chen, H.-Y., Kuo, L.-C., Lallemand, S.E., Tsien, H.H., 1997. Velocity field of GPS stations in the Taiwan area. Tectonophysics 274, 41–59.

Zhou, H.-W., 1994. Rapid three-dimensional hypocentral determination using a master station method. J. Geophys. Res. 99, 15439–15455.